2021-06-01

Effect of mixing ratios of natural inorganic additives in removing ammonia and sulfide in the liquid phase during anaerobic digestion of slaughterhouse waste

Mutegoa, Eric

Elsevier

https://doi.org/10.1016/j.mtchem.2020.100415

Effect of mixing ratios of natural inorganic additives in removing ammonia and sulfide in the liquid phase during anaerobic digestion of slaughterhouse waste

Article · January 2021

CITATIONS
0

READS
86

1 author:

Nyemaga Malima
Dodoma University
17 PUBLICATIONS **97** CITATIONS

SEE PROFILE

Materials Today Chemistry 20 (2021) 100415

Contents lists available at ScienceDirect

Materials Today Chemistry

journal homepage: www.journals.elsevier.com/materials-today-chemistry/

Effect of mixing ratios of natural inorganic additives in removing ammonia and sulfide in the liquid phase during anaerobic digestion of slaughterhouse waste

E. Mutegoa [a, b, *], N.M. Malima [b, c], A. Hilonga [a], K.N. Njau [d]

[a] Department of Materials, Energy Science and Engineering (MESE), School of Materials, Energy, Water and Environmental Sciences (MEWES), Nelson Mandela African Institution of Science and Technology, P.O. Box 447, Arusha, Tanzania
[b] Department of Chemistry, College of Natural and Mathematical Sciences (CNMS), The University of Dodoma, P.O. Box 338, Dodoma, Tanzania
[c] Department of Chemistry, University of Zululand, Private BagX1001, KwaDlangezwa, KwaZulu-Natal, South Africa
[d] Department of Water and Environmental Science and Engineering, School of Materials, Energy, Water, and Environmental Sciences (MEWES), Nelson Mandela African Institution of Science and Technology, P.O. Box 447, Arusha, Tanzania

ARTICLE INFO

Article history:
Received 13 September 2020
Received in revised form
16 December 2020
Accepted 18 December 2020
Available online xxx

Keywords:
Methanogenesis
Adsorption
Calcination
Total ammonia nitrogen
Sulfide

ABSTRACT

In this study, the efficacy of inorganic additives in the removal of total ammonia nitrogen (TAN) and sulfide in the aqueous phase of slaughterhouse waste undergoing anaerobic digestion in the batch reactor was investigated. A mixture of natural inorganic additives processed from the anthill and red rock soil samples collected from Arusha, Tanzania were used as adsorbents in different ratios. These materials were chosen in regard to their abundance in the local environment, surface properties, and elemental composition. Before analysis, the materials were pulverized and calcined at 700 and 900 °C for 2 h in a furnace and then sieved to 250 μm fine particle size. XRD analysis revealed that the anthill soil sample is endowed with major mineral phases of quartz and hematite while red rock soil contains albite, pyroxene, and quartz as predominant phases. The anthill and red rock soil samples calcined at 900 °C displayed higher BET surface areas of 815.35 and 852.35 m^2/g, respectively. The mixture of anthill soil and red rock soil in a ratio of 3:1 had a higher TAN removal efficiency of 92% at a contact time of 30 min compared to other ratios. On the other hand, a ratio of 1:2 showed a higher sulfide removal efficiency of 79% at a contact time of 60 min. Adsorption isotherm studies revealed that the Jovanovich model fitted better to the experimental data than the Langmuir and Freundlich models. The results demonstrated further that inorganic additives have a synergistic effect on stimulating methanogenesis as well as eliminating ammonia and sulfide during anaerobic digestion of slaughterhouse waste. Our findings demonstrate that anthill and red rock soils can be exploited as affordable, ecofriendly, and efficient adsorbents for mitigation of TAN and sulfide from the liquid phase and sustenance of methanogenesis.

1. Introduction

Anaerobic digestion (AD) refers to the process in which substrates with a high organic content are treated in the absence of oxygen to produce biogas [1]. Generally, biogas is a mixture of carbon dioxide and methane (50%–70%) along with other compounds such as ammonia, hydrogen sulfide, and siloxane in trace amounts [2]. Since the world is turning to alternative sources of energy from commonly used fossil fuels, biogas is regarded among the alternative sources of energy for domestic uses such as cooking and lighting. Unlike fossil fuel sources, which endanger the environment and ecosystem at large due to the excessive production of polluting agents, the use of alternative sources of energy has gained much attention due to the little waste, which is accumulated in the environment. As a substitute for fossil fuels, the use of biogas is regarded as an environmentally friendly technology to eradicate the emission of greenhouse gases, hence reducing climate warming [3]. In practice, AD has been used to produce biogas from various organic wastes due to their availability and as a means of waste management [4]. Both domestic and industrial activities have been the major source of tons of organic waste discharged in the environment, for which the biogas technology can be considered as the

* Corresponding author.
E-mail address: ericm@nm-aist.ac.tz (E. Mutegoa).

https://doi.org/10.1016/j.mtchem.2020.100415
2468-5194/

best solution to overcome their detrimental effects on the environment [5]. Organic wastes such as domestic leftovers [6], cow dung [7], industrial waste [8], municipal solid waste [9], agro waste [10], and abattoir waste [11], to mention a few, are a good source to generate biogas due to their high carbon/nitrogen ratio. The higher C/N ensures the sustainability of microorganisms and a proper balance of nutrient ratio between carbon and nitrogen, in which a high carbon content favors the maximum production of methane gas [12]. For example, more than 50% of the total meat consumption in Tanzania is from beef cattle, which accumulates a lot of waste during meat processing [13]. This situation presents a need to utilize the particular waste as a means of resource recovery and waste management. Hence, batch reactors loaded with slaughterhouse waste were set for an experiment during this study. The selection of the substrate was based on its high composition of proteins and lipids mixed with its water content [14]. In that case, slaughterhouse waste is regarded as a potential substrate for methane production during the AD process. The breaking down of carbon-rich substrates by microorganisms during AD is sometimes associated with the emission of unwanted contaminants in the digester, which are considered toxic to microorganisms. Additionally, the excess production of other intermediate products such as siloxanes, halogens, ammonia, aromatics, hydrogen sulfide, and volatile organic compounds can result in digester failure due to the inhibition process, which particularly affects methanogens [15,16]. Since slaughterhouse waste is composed of animal fats and protein components of blood, the digestion process breaks down both cysteine and methionine, which results in the formation of sulfur [17]. Therefore, free ammonia is also accumulated in the aqueous phase because of a high nitrogen content resulting from protein decomposition, while long-chain fatty acids accumulate as a result of fat degradation [18]. The presence of both sulfur and ammonia in the liquid phase becomes inhibitory to methanogens during the AD process, and as a result, the quality of biogas produced decreases. The inhibition occurs as a result of competition between sulfur-reducing bacteria and methane-producing archaea by oxidizing molecular hydrogen at a high chemical oxygen demand (COD) value [19]. It is reported that the total ammonia nitrogen (TAN) in the range of 1500–5000 mg/L is inhibitory to microorganisms during biological treatments [20]. Nonetheless, the concentration of ammonia nitrogen (NH_3–N) above 2 mg/L can be toxic to aquatic species at a certain range of pH, temperature, and other parameters [21]. Similarly, total sulfide ($HS^- + H_2S$) in the range of 100–800 mg/L is also reported to be inhibitory to methanogens as it suppresses methane production [22]. Several physical–chemical and biotechnological approaches such as ion exchange, struvite precipitation, membrane distillation, adsorption additives, C/N ratio adjustment, and nitrification–denitrification methods have been applied to lower the concentrations of sulfide and ammonia in the liquid phase during the AD process [23,24]. However, a physical–chemical method, which involves the use of various additives with high affinity to ammonia and sulfide, has been dominating over the other methods due to its high removal efficiency and affordability [25]. This method involves the adsorption process in which the surface of the adsorbent attracts adsorbate molecules due to intermolecular forces. The process eventually results in the formation of a new chemical bond at the adsorbent's surface as a result of chemical interaction between the surface of the adsorbent and the adsorbate [26]. Several adsorbents have been applied by researchers, for example, zeolites for the removal of both forms of ammonia (NH_3 and NH_4^+) and iron-rich materials such as iron pellets for hydrogen sulfide removal [27,28]. Furthermore, adsorption by activated carbon has been reported to have a relatively low adsorption capacity of about 6.079 mg/g in removing ammonia from aqueous solutions [29]. Generally, most of the materials that are already existing are industrially synthesized, which are readily expensive and unaffordable to apply for the removal of contaminants in the liquid phase. It is therefore recommended that economically feasible methods be employed for lowering both ammonia and sulfide inhibition in order to elevate the methane content produced during the AD process. In this study, affordable and readily available inorganic materials rich in hematite and aluminosilicate were employed in different stoichiometric amounts for both ammonia and sulfide removal in the liquid phase during AD of slaughterhouse waste. In addition, the effect of the adsorbent mixture on the methanogenesis process was also investigated by measuring the content of methane produced in relation to the accumulation of volatile fatty acids and alkalinity in the reactor. Moreover, the influence of calcination temperature on the physicochemical properties of the adsorbent materials was also examined. The selection of anthill and red rock soil samples was based on their elemental composition such as iron in the form of magnetite (Fe_3O_4) and hematite (Fe_2O_3) [28]. These iron contents are considered as remaining products of rocks that have undergone leaching and oxidizing practices during the weathering process. The presence of iron oxide in the red soil is a major breakthrough for the precipitation of sulfide into elemental sulfur [30]. Meanwhile, the high amount of alumina (Al_2O_3) and silica (SiO_2) composing the aluminosilicate cage in anthill soil provides a means for removing ammonia/ammonium (NH_3/NH_4^+) from the substrate undergoing the AD process through ion exchange and adsorption processes [31].

2. Materials and methods

2.1. Sample collection, pretreatment, and preparation

The substrate used in this experiment was a liquid mixture of blood and intestine discharged from a slaughterhouse waste point owned by Arusha Meat Company Limited, located in Arusha City, Tanzania. The sample was then stored in a fridge at 4 °C before characterization. The substrate stored was inoculated with 10% (w/v) of cow dung, which was obtained from cattle keepers. The mixture was then fed into a batch-reactor of 1 L capacity for biogas production. Adsorbent materials used in this study were soil samples obtained from two different locations. The red rock soil sample was collected from the Nayobi village, Ngorongoro district, Arusha, Northern Tanzania, whereas the anthill soil sample was collected from an anthill around the campus of Nelson Mandela African Institution of Science and Technology (NM-AIST), Arusha, Tanzania. The two types of soil samples were processed into powder form before further analysis. The red rock was pulverized to 250 μm fine particles and calcined in the furnace (Thermo Scientific 1200 Box Furnace) at 700 and 900 °C for 2 h. The calcined samples were allowed to cool to room temperature and processed further by grinding and sieving using sieve no.16 of 250 μm before further analysis. Similar procedures were followed to process the anthill soil sample. The obtained calcined adsorbent materials were kept in a clean container and labeled as AHX and RRX, where the prefixes 'AH' and 'RR' denote anthill and red rock respectively. The postscript 'X' represents the calcination temperature.

2.2. Analytical methods

Both total solids (TS) and volatile solids (VS) were determined by using the standard protocols for wastewater examination [32]. A HACH DR2800 instrument (HACH, Loveland, CO) was used to measure the chemical oxygen demand (COD) value using HACH

digestion solution vials for high range COD (20 mg/L to 1500 mg/L) following the manufacturer's protocol [33]. On the other hand, the biological oxygen demand (BOD_5) value was also measured using the OxiTop method in which the stored values were quantified in mg/L after 5 days. All measurements for both COD and BOD were performed in triplicate. The Ripley and Kapp titration methods were used to determine the concentrations of volatile fatty acids (VFA) and alkalinity [34]. The pH of the samples was measured using a VWR symphony pH meter. The concentrations of TAN and sulfide in the liquid phase were ascertained by the Nessler method and methylene blue method, respectively [35,36]. Liquid samples were collected and then centrifuged at 8000 rpm for 15 min and then filtered through a 0.45 μm Whatman filter paper. The filtrate collected was then used to measure the parameters such as pH, VFA, total ammonia, and alkalinity. Methane content was determined using a biogas analyzer i.e. Geotec Biogas 5000. The summation of both unionized [NH_3–N] and ionized [NH_4^+] forms of ammonia was used to quantify the TAN by equation (1) given below [37]:

$$[TAN] = [NH_3] + [NH_4^+] \quad (1)$$

The adsorption capacity was calculated using a mass balance according to equation (2), which is given below:

$$Q_e = \frac{(C_o - C_e)V}{m} \quad (2)$$

where Q_e is the mass of TAN/S^{2-} exchanged per unit mass of adsorbent mixed at different ratios (mg/g), C_0 and C_e are initial and equilibrium concentrations of TAN/S^{2-} in the liquid phase (mg/L), respectively, V is the volume of the slurry mixture (L), and m is the mass of the adsorbent (g).

The adsorbate (TAN and S^{2-}) removal efficiency was calculated using equation (3) given below:

$$\text{Removal efficiency } (\%) = \frac{(C_o - C_e)100}{C_o} \quad (3)$$

where C_0 (mg/L) is the initial concentration of TAN/S^{2-} in the liquid phase and C_e (mg/L) represents the equilibrium concentration of TAN/S^{2-} in the liquid phase. All these laboratory analyses were carried out at the Nelson Mandela African Institution of Science and Technology (NM-AIST), Arusha, Tanzania.

2.3. Adsorbent characterization

The mineral phases present in the adsorbent materials were elucidated by employing powder-X-ray diffraction (p-XRD). The analyses were performed in the high angle 2θ ranging from 5 to 55° using a Bruker AXS D8 Advance X-ray diffractometer equipped with a nickel-filtered Cu Kα radiation (λ = 1.7890 Å) at 40 kV, 40 mA, and room temperature. The scan speed was 0.5 s/step at an increment of 0.01314. The textural properties of both red rock and anthill soil samples were analyzed using the Brunauer–Emmett–Teller (BET) method to determine the specific surface area while pore size and pore volume were evaluated using the Barrett–Joyner–Halenda (BJH) method. Nitrogen adsorption–desorption isotherms were assessed at 77 K by using a porosimeter (Nova 4200e Quantachrome, UK) after degassing the sample at 160 °C for 3 h. About 0.1 g of the calcined soil sample was used for an adsorption–desorption process at a temperature of −195.8 °C. The infrared spectroscopy measurements (FT-IR, Perkin–Elmer, Spectrum 100) were carried out to identify the vibration frequency in the functional groups of the adsorbent materials. The wavelength of the spectra was obtained in the range of 400 and 4000 cm^{-1}. The sample's chemical composition was determined at the Geological Survey of Tanzania (GST) using an X-ray fluorescence analyzer (XRF), model Vanta Element Series manufactured by Olympus Scientific Solutions, USA. The surface microstructure and morphology of the calcined samples (AHX) and (RRX) were investigated using a Zeiss Ultra Plus Field Emission Scanning Electron Microscope (FE-SEM) from The University of Cape Town, South Africa.

2.4. Experimental setup

In this experiment, side-arm conical flasks (Pyrex) of 1 L capacity fed with slurry (a mixture of abattoir waste and 10% w/v cow dung inoculum) to about 900 mL were used as batch reactors. The remaining 100 mL was used as headspace volume. The reactors were immersed into three thermostat water baths operated at 37 °C and labeled as A, B, and C. Each of the three thermostat water baths was equipped with three reactors. Reactors in water bath A were used as the control of the experiment, which was run in triplicate. The reactors in the respective water baths were named as A1, A2, and A3; B1, B2, and B3; and C1, C2, and C3. Each reactor was connected to a 1 L Tedlar gas sampling bag. Then, the experiment was run, and the AD was allowed to proceed for 65 days to monitor the level of ammonia and sulfide inhibition as well as methane production before and after the addition of inorganic additives for the adsorption process. Shaking of reactors was done twice a day at 10:00 a.m. and 10:00 p.m. After 44 days of the initial AD process, adsorbent materials (AHX and RRX) for adsorption of TAN and sulfide concentrations were applied in each reactor at the mixed ratios of 1:1, 1:2, and 3:1 (AH:RR). This was followed by another 20 days of monitoring the removal efficiency and the impact of each reactor composition on methane production. Unlike reactors in water bath A, which were used as a control experiment, those in water bath B and C were supplied with adsorbent materials calcined at 700 and 900 °C, respectively. The adsorbent material (4 g) was contacted with 1 L of the substrate containing the adsorbate under study. The resulting mixture was shaken well for 5 min. Thereafter, the removal efficiencies for TAN and S^{2-} were recorded at intervals of 5, 10, 15, 20, 30, 60, 90, and 120 min. Measurements of other parameters such as (NH_3/NH_4^+), alkalinity, VFA, pH of the slurry, and methane content were carried out after every 7 days.

2.5. Adsorption isotherm studies

The adsorption capacities for the uptake of TAN and sulfide by the AH@RR adsorbent were studied using the Langmuir (4), Freundlich (6), and Jovanovich (7) isotherm models in accordance with experimental data. The equilibrium behavior of TAN and sulfide exchange with the adsorbents in different ratios was characterized by fitting the model equations to the experimental data. The Langmuir adsorption assumes that the adsorbent's surface is uniform (monolayer) with no interaction between adsorbed and desorbed molecules, which exist in equilibrium. On the other hand, the Freundlich isotherm describes the existence of multisite adsorption on rough (heterogeneous) surfaces. In the Jovanovich model, the assumptions considered are the same as in the Langmuir model. However, the possibility of mechanical contact between the adsorbent and adsorbates is mostly taken into consideration in this model [38,39].

The linear Langmuir equation is written as:

$$\frac{C_{eq}}{q_e} = \left(\frac{1}{q_{max}}\right)C_{eq} + \frac{1}{k_L q_{max}} \quad (4)$$

where q_e (mg/g) is the amount of TAN/S^{2-} adsorbed at equilibrium, q_{max} (mg/g) is the maximum adsorption capacity, C_{eq} (mg/L) is the

concentration at equilibrium, and k_L (L/mg) is the Langmuir equilibrium constant.

$$R_L = \frac{1}{1 + K_L C_o} \quad (5)$$

The linear Freundlich equation is written in the following form:

$$q_e = k_f . C_{eq}^{1/n} \quad (6)$$

where q_e (mg/g) is the amount of TAN/S^{2-} adsorbed at equilibrium, C_{eq} (mg/L) is the concentration at equilibrium, k_f (mg/g) is the Freundlich capacity coefficient, and 1/n is the measure of adsorption intensity. However, equation (6) above is further deduced to equation (7) below for quantification of parameters.

$$\log q_e = \frac{1}{n} \log C_{eq} + \log k_f \quad (7)$$

The linear Jovanovich equation is written in the following form:

$$\ln q_e = \ln q_{max} - K_J C_{eq} \quad (8)$$

where q_e (mg/g) is the amount of TAN/S^{2-} adsorbed at equilibrium, q_{max} (mg/g) is the maximum adsorption capacity, C_{eq} (mg/L) is the concentration at equilibrium, and K_J (l/g) is the Jovanovich constant.

3. Results and discussion

3.1. Substrate characterization

The substrate mixture was characterized before being introduced into the reactor for analyzing the parameters such as TS, VS, COD, and BOD. The values of TS, VS, COD, and BOD in the raw substrate were found to be 0.93%, 78.09%, 11,025, and 1600, respectively. Characterization was also performed after 65 days of the digestion process where the values of TS, VS, COD, and BOD were found to be 3.59%, 68.12%, 1575, and 375 respectively. The VS removal efficiency at day 65 was 12.77%. The increase in TS was due to the addition of inorganic additives in the reactor at day 44 of AD.

3.2. Adsorbent characterization

3.2.1. XRD analysis

The XRD analysis was performed to ascertain the mineral phases present in both anthill and red rock soil samples, and the profiles for both samples are presented in Fig. 1. From the XRD spectra, it was observed that the anthill soil sample (AH) contains quartz (SiO_2), as a dominant phase followed by hematite (Fe_2O_3). In addition to the two major phases, traces of cristobalite (SiO_2) and pyroxene-ideal ($MgSiO_3$) were found to be present. The peaks for quartz appears at 2θ = 25.39°, 32°, and 47.6° corresponding to d = 4.07, 3.25, and 2.22 Å, respectively, while those for hematite appears at 2θ = 28.1°, 38.84°, and 41.71° corresponding to d = 3.67, 2.69, and 2.51 Å, respectively. The diffraction peaks for trace minerals were identified as follows: cristobalite (2θ = 24.85° and 41.12° for d = 4.16 and 2.55 Å) and pyroxene ideal (2θ = 23.07°, 32°, 36.12°, 41.12°, and 47.6° corresponding to d = 4.47, 3.24, 2.88, 2.54, and 2.21 Å, respectively). On the other hand, the XRD profile of RR soil confirmed the presence of albite ($Al_{1.02}Ca_{0.02}Na_{0.98}Si_{2.98}O_8$) as the dominant phase followed by pyroxene ($Al_{1.38}Ca_{0.74}Fe_{0.16}Mg_{0.01}Si_{1.5}O_6$), quartz ($SiO_2$), stishovite ($SiO_2$), and hematite ($Fe_2O_3$). Traces of downeyite ($SeO_2$), halite (NaCl), magnetite, and witherite ($BaCO_3$) were also observed. The diffraction patterns of the dominant albite phase were observed at 2θ = 25.65°, 27.56°, 28.11°, 29.85°, 31.0°, 32.3°, 34.80°, 35.39°, 38.72°, 40.90°, 41.62°, 47.0°, 49.05°, and 52.0° corresponding to d = 4.02, 3.75, 3.68, 3.47, 3.34, 3.21, 2.99, 2.94, 2.69, 2.56, 2.51, 2.24, 2.15, and 2.04 Å, respectively. The pyroxene phase registered its peaks at 2θ = 28.11°, 31.0°, 32.3°, 34.8°, 35.39°, 35.96°, 40.90°, 41.62°, and 47.78° at d = 3.68, 3.34, 3.21, 2.99, 2.94, 2.89, 2.56, 2.51, and 2.20 Å, respectively, while peaks for quartz were found at 2θ = 24.97°, 32.30°, 47.78°, 49.05°, and 52° at d = 4.13, 3.21, 2.20, 2.155, 2.04 Å, correspondingly. The peaks for other phases were also found within the same range of diffraction angle of 2θ = 35.39° and 47° at d = 2.94 and 2.2 4 Å (stishovite), 2θ = 28.11°, 38.72°, 41.62°, and 47.78° at d = 3.68, 2.69, 2.51, and 2.20 Å (hematite), 2θ = 34.80° and 40.90° at 2.99 and 2.56 Å (magnetite), 2θ = 27.56°, 28.11°, 38.72°, 47.0°, 47.78°, 49.05° and 52.0° at d = 3.75, 3.68, 2.69, 2.24, 2.20, 2.15, and 2.04 Å (witherite), 2θ = 31.0°, 35.39°, and 52.0° at d = 3.34, 2.89, and 2.04 Å (halite), and 2θ = 24.97°, 27.56°, 32.30°, 34.80°, 41.62°, and 49.05° at d = 4.13, 3.75, 3.21, 2.99, 2.51, and 2.15 Å (downeyite), respectively. The diffraction patterns of the phases present in the anthill and red rock soil samples are in agreement with the standard diffraction patterns of the respective phases reported in the literature [40–47].

3.2.2. Analysis of chemical composition

The XRF results of AH and RR samples are displayed in Table 1. It is observed that the AH soil has a higher amount of alumina (36.15%), which is greater than the amount of all other chemical

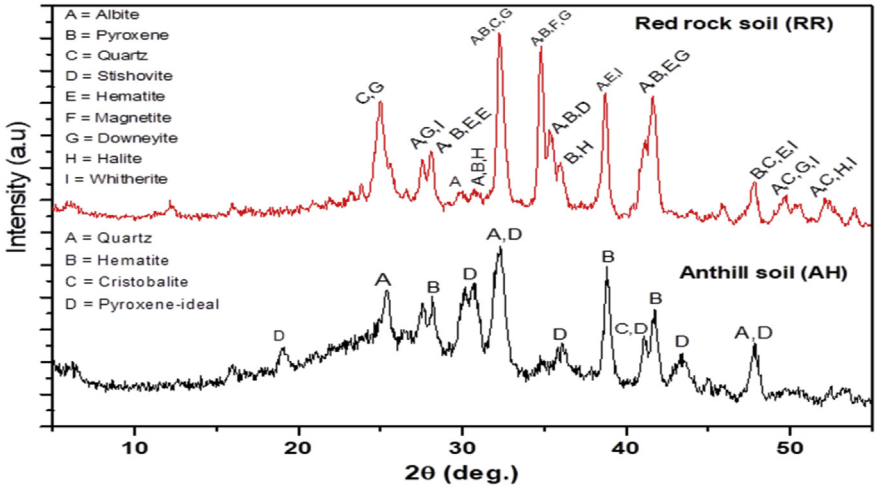

Fig. 1. XRD spectra of anthill (AH) and red rock (RR) soil samples.

components. In addition, the presence of both Al_2O_3 (36.15%) and SiO_2 (16.83) confirms the aluminosilicate nature of the soil. Similarly, RR soil contains high proportions of SiO_2 (31.33%) and Al_2O_3 (23.23%). Since silica and alumina are vital components of both the soil samples, an elegant mixture of the two soil samples coupled with their synergism is expected to enhance the removal efficiency of pollutants in the substrate undergoing the AD process. Besides the alumina and silica contents, both soil samples have an appreciable content of hematite (Fe_2O_3), which is a key component for the precipitation of sulfides. Furthermore, the loss on ignition (LOI), which is an index measure of the organic content of the soil, shows that anthill soil has a high amount of volatile content than red rock soil. The LOI for anthill soil is enriched by the buildup of a distinct surface crust during heating that insulates the core of the sample from ignition temperatures [48]. Generally, the compositions of the two soil samples in terms of relative weights were found to be in good agreement with the major phases obtained from the XRD analysis.

3.2.3. FTIR analysis

The functional groups of the sorbent materials were analyzed by Fourier transform infrared spectroscopy, and the results are displayed in Fig. 2. The FT-IR spectra indicate the presence of the Si—O— group at the surfaces of both AH and RR materials. Silanol groups (Si OH) are formed due to the fragmentation of silica surfaces and are commonly available on the surface of the adsorbent material due to the presence of silica (SiO_2) as reflected in the XRF results (Table 1). In both anthill and red rock soil samples, the broad bands assigned for Si—O— were observed around 1000 cm^{-1}. The other species that may be present on the silica surface is hydrogen-bonded to silanol groups, which are significant for enhancing the adsorption process through interaction with the adsorbates.

3.2.4. Analysis of BET surface area and porosity characteristics

The calcination of aluminosilicate materials is essential for the volatilization of the organic template and condenses the silanol groups present in the silicate cage. The process enhances the surface area and micropore volume and exposes the silanol groups at the surface of the adsorbent material for improving the adsorption capacity. Results in Table 2 indicate that the surface areas of both anthill and red rock soil samples were obtained at higher calcination temperatures. The anthill soil calcined at 700 and 900 °C developed surface areas of 613.88 and 815.35 m^2/g, respectively. Meanwhile, the red rock soil developed surface areas of 601.43 and 852.8 m^2/g at 700 and 900 °C, respectively. In addition, the pore volume for the anthill soil sample increased from 0.51 cm^3/g at 700 °C to 1.21 cm^3/g at 900 °C. Likewise, the pore volume for red rock soil augmented from 0.62 cm^3/g at 700 °C to 0.75 cm^3/g at 900 °C. Furthermore, the pore diameter for both anthill and red rock soil samples seemed to increase with the calcination temperature. For instance, the anthill soil calcined at 700 °C recorded a pore diameter of 15.19 Å, which increased to 15.22 Å at 900 °C. On the other hand, the pore size of the red rock soil sample increased from 15.17 Å at 700 to 30.49 Å at 900 °C.

The effect of calcination of the adsorbent materials is further manifested by N_2 adsorption–desorption and micropore development. As a result of calcining anthill soil at 900 °C, it was possible to achieve higher N_2 adsorption with the highest possible pore volume of 816.32 cm^3/g and a relative pressure of 0.99 P/P_0 (Fig. 3b). Similarly, red rock soil calcined at the same temperature attained higher N_2 adsorption with the pore volume of 515.85 cm^3/g at a relative pressure of 0.99 P/P_0 (Fig. 3d). This implies that the calcination process favored the formation of both micropores and mesopores in both the adsorbent materials. Since anthill soil exhibited a higher N_2 adsorption capacity than red rock soil, it is therefore agreed that anthill soil has a higher pore volume and sufficient surface area features than red rock soil. This means that anthill soil has efficient adsorption properties compared to red rock soil.

Table 1
Chemical composition of AH and RR analyzed by XRF.

Sample ID	SiO_2 (%)	CaO (%)	MgO (%)	Fe_2O_3 (%)	Al_2O_3 (%)	Na_2O (%)	LOI
AH	16.83	1.61	1.51	12.14	36.15	–	16.52
RR	31.33	9.54	7.79	14.38	23.23	9.14	4.42

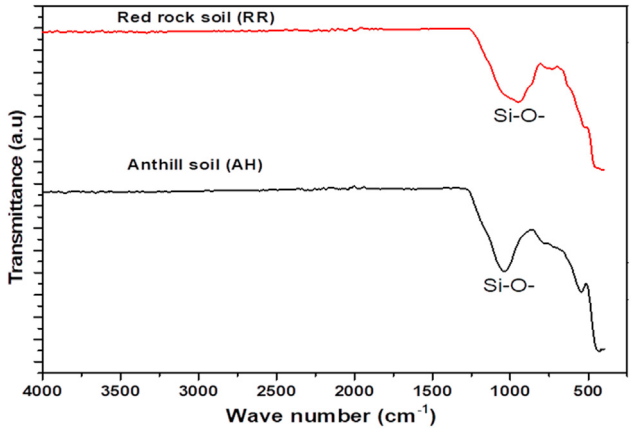

Fig. 2. FTIR spectra of AH and RR.

3.2.5. Morphological analysis

The surface morphologies of AH and RR adsorbents calcined at 700 °C and 900 °C were ascertained by FE-SEM, and the micrographs are displayed in Fig. 4. It can be seen that the adsorbent displays small hollow multipores, which are likely to contribute to the increase in the surface area. The agglomeration of particles is also obvious in the adsorbent material. The observed agglomeration of the adsorbent materials can be attributed to the magnetic interaction among the hematite/magnetite components of the materials, where each magnetic particle behaves like a magnet [49]. The extent of agglomeration is observed to increase with the calcination temperature, a phenomenon that enhances high uptake of TAN and sulfide contaminants in the liquid phase.

3.3. Determination of parameter composition of slaughterhouse waste undergoing AD

In the course of AD of slaughterhouse waste, different parameters such as VFA, alkalinity, pH, and TAN, sulfide, and methane concentrations were determined in both control experiment and after the addition of the adsorbents. From the results in Table 3,

Table 2
BET surface area, pore size, and pore volume for AH and RR samples.

	Surface area (m^2/g)	Pore volume (cm^3/g)	Pore diameter (Å)
Anthill soil			
AH700	613.88	0.51	15.19
AH900	815.35	1.21	15.22
Red rock soil			
RR700	601.43	0.62	15.17
RR900	852.8	0.75	30.49

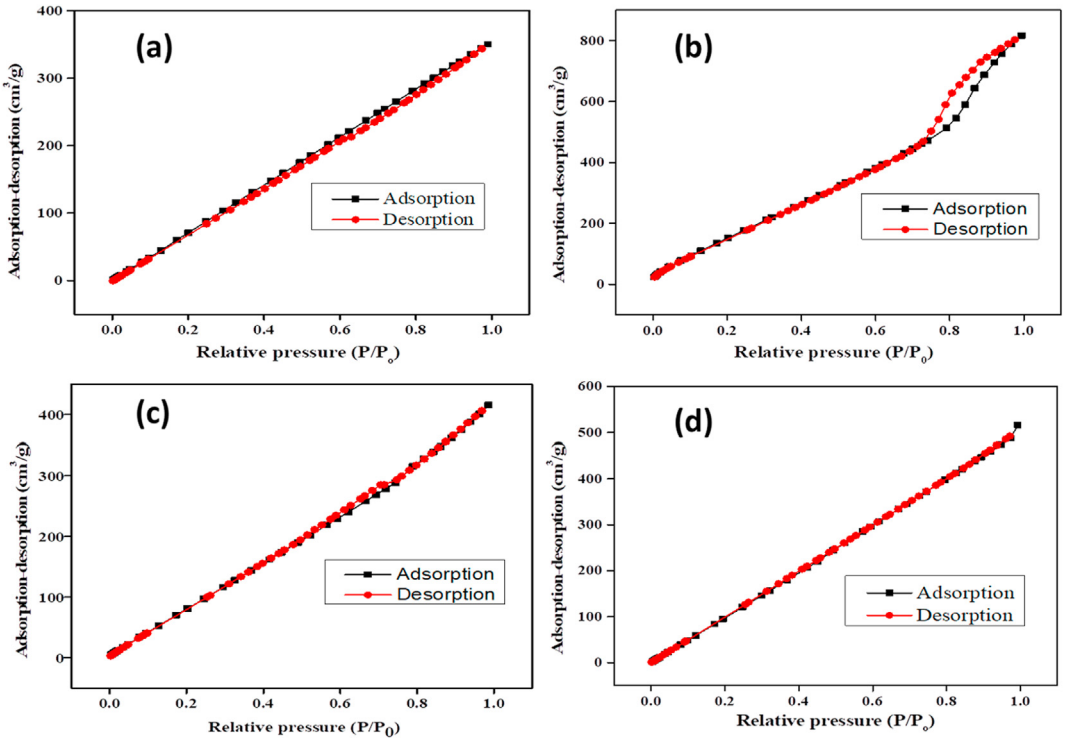

Fig. 3. Adsorption–desorption isotherms of (a) AH700, (b) AH900, (c) RR700, and (d) RR900.

notably a control experiment, the TAN level (obtained with the aid of Eq. (1)) was increasing throughout the digestion process, though there was a decrease in VFA concentration, which is regarded as food for methanogens [50]. The increasing trend of TAN affected methane production from day 37 to day 44, leading to a decrease in methane content by 35.9%. However, the decrease in methane content was further observed throughout the AD process as the amount of TAN increased. From Table 3, the minimum concentration of TAN was recorded to be 1022.64 ± 0.95 mg/L on day 22 and increased tremendously as the degradation process was proceeding. The amount of TAN recorded was far above the recommended level for methanogens to resist the inhibition process. This is supported by the fact that the TAN concentration in the range of 1000–1500 mg/L is often regarded as the key factor for inhibition and AD failure in general [51]. This indicates that the methanogenesis stage was highly affected due to the inhibition process attributed to a higher concentration of TAN. The ratio between VFA and alkalinity can be considered as an essential parameter to describe the digester's performance at mesophilic temperature. Since VFA is regarded as food for methanogens during fermentation [52], its decrease is associated with the total breakdown of the organic content by microorganisms. However, the VFA/alkalinity ratio produced between day 26 (0.39) and day 44 (0.31) is within the recommended threshold value of 0.3–0.4 [53], for a stable biodigester with a pH range of 7.5–7.6. For instance, the highest methane content of about 55.7% was recorded during day 37 in which the VFA/alkalinity ratio was 0.34 as indicated in Table 3. Nevertheless, from day 37 onwards, the control experiment showed a decrease in the threshold value as the TAN concentration was increasing. This phenomenon, coupled with the inhibition process induced by high accumulation of TAN concentration, resulted in the decrease of methane content.

3.4. Adsorption of TAN and sulfide by the AH@RR adsorbent

3.4.1. Determination of adsorption capacity (mg/g) and removal efficiency (%)

The removal efficiencies for both TAN and sulfide in the liquid phase were estimated using Eq. (3) based on the mixing ratios of anthill and red rock soil adsorbents. The AH to RR adsorbent ratios were 1:1, 1:2, and 3:1 for TAN adsorption and 1:1 and 1:2 for sulfide adsorption. From the results indicated in Fig. 5a, it is clear that the removal efficiency for TAN did not show any clear order based on the calcination temperature of the adsorbent mixture, surface area, and pore volume distribution. For instance, the ratio of 3:1 for the adsorbent mixture calcined at 700 °C exhibited a higher removal efficiency (92%) for TAN than the same ratio of adsorbent mixture calcined at 900 °C (82%), which was observed to possess high surface area and porosity behavior. However, the ratio of 1:2 of the adsorbent mixture calcined at 900 °C showed a high removal efficiency for sulfide (82%) compared to the same ratio of adsorbent mixture calcined at 700 °C, which showed a removal efficiency of 79%. As opposed to TAN, the higher sulfide removal shown by the adsorbent mixture in the ratio of 1:2 calcined at 900 °C is in agreement with the results of improved physicochemical characteristics such as surface area and porosity features of the adsorbent as a result of a higher temperature calcination. In addition, the higher sulfide removal efficiency demonstrated by the adsorbent ratio of 1:2 is ascribed to the appreciable content of hematite (Fe_2O_3), which influenced the precipitation reaction of iron sulfide. Thus, the adsorption of TAN onto the adsorbent mixture calcined at both 700 and 900 °C followed the 3:1 > 1:1 > 1:2 trend (Fig. 5a), whereas the trend for sulfide removal efficiency is 1:2 > 1:1 (Fig. 5b). From these trends based on different mixing ratios, it is obvious that the higher mixing ratio of anthill soil is sufficient for

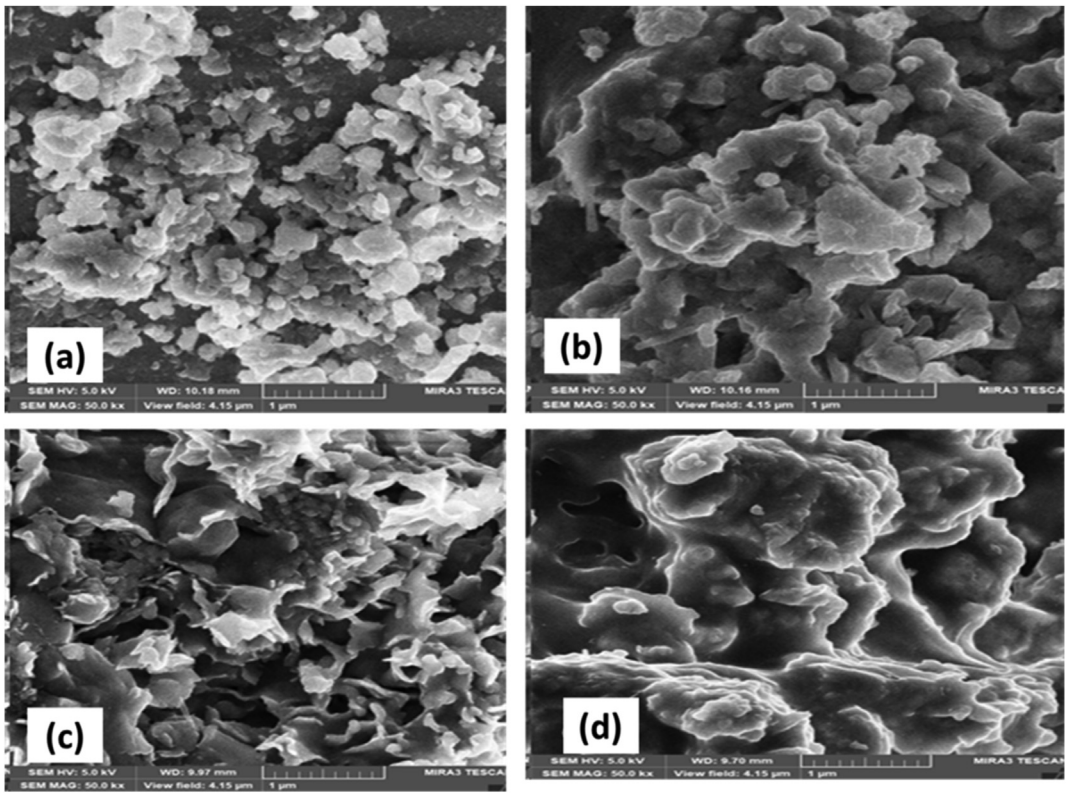

Fig. 4. SEM images of (a) AH700, (b) AH900, (c) RR700, and (d) RR900.

Table 3
Parameter analysis of slaughterhouse waste before and after adsorption during the AD process.

	Control experiment							Parameters assessed after addition of adsorbents		
	VFA (mg/L)	Alkalinity (mg/L)	Ratio (VFA/Alk)	TAN (mg/L)	S^{2-}(mg/L)	%CH_4	pH	VFA	%CH_4	pH
Day 1(in)	152.89 ± 2.22	202.23 ± 3.25	0.76	1041.03 ± 2.59	32.54 ± 0.59	–	7.70			
Day 8	210.5 ± 2.1	285.32 ± 4.71	0.74	1029.38 ± 2.38	27.20 ± 0.66	29.2	7.69			
Day 15	270.45 ± 0.70	495.73 ± 5.49	0.55	1030.04 ± 1.05	13.41 ± 0.74	41.2	7.65			
Day 22	390.85 ± 5.94	819.77 ± 3.53	0.48	1022.64 ± 0.95	9.610 ± 1.04	54.3	7.50			
Day 26	304.51 ± 6.16	786.99 ± 4.83	0.39	1035.79 ± 1.56	14.51 ± 0.64	52.8	7.51			
Day 37	274.41 ± 7.39	804.24 ± 5.81	0.34	1093.81 ± 2.78	10.51 ± 0.45	55.7	7.42			
Day 44	252.40 ± 4.85	811.59 ± 2.48	0.31	1111.91 ± 1.53	12.41 ± 0.35	35.7	7.24			
Day 51	173.16 ± 2.36	821.56 ± 4.15	0.21	1109.43 ± 1.09	14.93 ± 0.15	28.2	7.18	152.24	41.0	7.31
Day 58	142.48 ± 3.5	847.96 ± 4.91	0.17	1109.79 ± 1.95	11.31 ± 0.06	24.6	7.06	122.54	48.4	7.42
Day 65	135.09 ± 2.43	938.74 ± 4.47	0.14	1210.17 ± 0.71	10.28 ± 0.24	22.8	7.10	112.82	60.3	7.50

the removal of TAN with almost 90% removal efficiency regardless of the calcination temperature. Moreover, the higher mixing ratio of the red rock soil sample seemed to perform better in removing sulfide in the liquid phase, with almost 80% removal efficiency. The results of this study are comparably higher or within the range of previous studies on other adsorbents in removing TAN and sulfide in the liquid phase [54,55]. Nevertheless, the frequent use of ferric and ferrous salts (Fe^{3+}/Fe^{2+}), which oxidizes sulfur, has been commonly practiced in which the combined species has depicted a higher removal efficiency for sulfide in the aqueous phase than when either of the species is used alone [56]. Farghali and other co-authors have indicated that the reduction of hydrogen sulfide (H_2S) can be achieved in the range of 83.82–98.10% from day 10 during AD of cattle manure through direct application of metal oxide nanoparticles [57]. The present study, however, has demonstrated the use of local powder processed from cheap and abundant inorganic materials collected from the Northern Zone of Tanzania, for the removal of ammonia and sulfide in the liquid phase.

In addition to the removal efficiency (%), the adsorption capacity (mg/g) of different ratios of the adsorbent mixture was determined using Eq. (2), and the results are presented in Fig. 6. For example, Fig.6a indicates that the ratio of AH to RR of 1:1 for the adsorbent mixture calcined at 700 °C is superior for TAN adsorption to the other ratio mixtures. This implies that the 1:1 mixture takes up a higher amount of TAN per unit mass of AH@RR. A similar trend for sulfide removal is also observed for the same adsorbent mixture calcined at 700 °C (Fig. 6b). Generally, the overall trend in TAN removal capacities by different ratios of adsorbent mixtures calcined at both 700 and 900 °C follows the following sequence: 1:1 > 3:1 > 1:2 °C, while the trend for sulfide removal follows the 1:1 > 1:2 sequence. From the trends of both TAN and sulfide removal capacities, it is evident that the ratio of 1:1 for the adsorbent mixture calcined at 700 °C was more efficient than all other mixing ratios. Similar observations have been reported for most of the adsorbents calcined at temperatures ranging from 500 to 700 °C, showing high adsorption capacities [58].

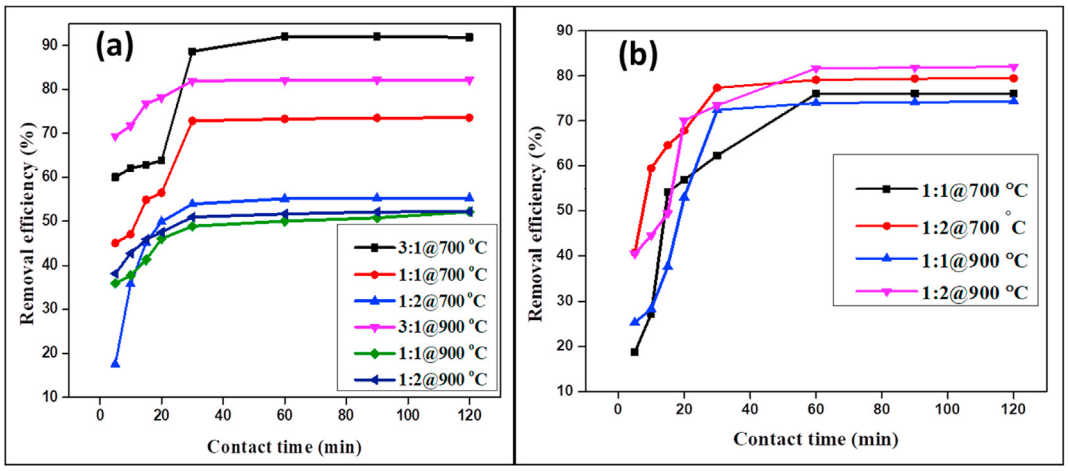

Fig. 5. Removal efficiencies for (a) TAN and (b) sulfide at different ratios of adsorbent mixture calcined at 700 and 900 °C.

3.4.2. Effect of adsorption time on the removal efficiency

The contact time between the adsorbent and adsorbate is important in determining the adsorption equilibrium. In this study, the removal efficiency of the AH@RR adsorbent was studied by varying the adsorption time from 0 to 120 min. As seen from Fig. 5a, all the ratio mixtures have shown maximum removal efficiency for TAN within the first 30 min; thereafter, little changes on the removal efficiency were recorded, followed by a steady adsorption process. On the other hand, the maximum removal of sulfide was achieved during the first 60 min, after which a constant adsorption process was observed (Fig. 5b). This implies that the adsorption equilibrium was attained during the first 30 min for TAN and 60 min for sulfide under the given conditions and maximum removal efficiency had taken place. This fast adsorption process may be ascribed by the fast migration of adsorbate molecules resulting from abundant active adsorption sites on the surface of AH@RR. After equilibrium, the observed steady adsorption is related to the buildup of adsorbate molecules on the adsorbent surface, hence blocking further adsorption of extra molecules to the existing active sites. There are reports on the use of other adsorbent materials in removing TAN and sulfide from environmental matrices. However, most of these adsorbents took a longer contact time to reach equilibrium compared to the mixture of adsorbents used in this study. This variation of contact time is attributed to differences in particle size, experimental conditions, and surface properties of the sorbent materials. For instance, the study by Njoroge and Mwamachi [59] revealed that natural zeolite could even take more than 120 min for the uptake of ammonia with a removal efficiency of 50%. Sébastien Ryskie and colleagues [60] used ozone microbubbles to evaluate their performance in removing ammonia nitrogen (NH_3—N) in a batch mode. In their study, the removal efficiency in the range of 27.8–99.3% was recorded after a treatment period of 570 min. The results on the variation of adsorption efficiency as a function of contact time obtained in this study are a major breakthrough for industrial application because fine adsorbent particles like powdered AH@RR tend to equilibrate with sorbate particles at a very shorter time.

3.4.3. Adsorption isotherm studies

The Langmuir, Freundlich, and Jovanovich isotherm models were studied to evaluate the interaction behavior between active sites of AH:RR surfaces and the adsorbate particles. These isotherm models provide the correlation between the equilibrium amount of TAN and sulfide in the liquid phase and that in the adsorbent phase. The Langmuir isotherm parameters summarized in Table 4 were computed by using equations (4) and (5) to give the plots shown in Fig. 7a and b. The slope and intercept of the linearized Langmuir plots of C_e/q_e vs. C_e were used to obtain the values of q_m, K_L, R_L, and

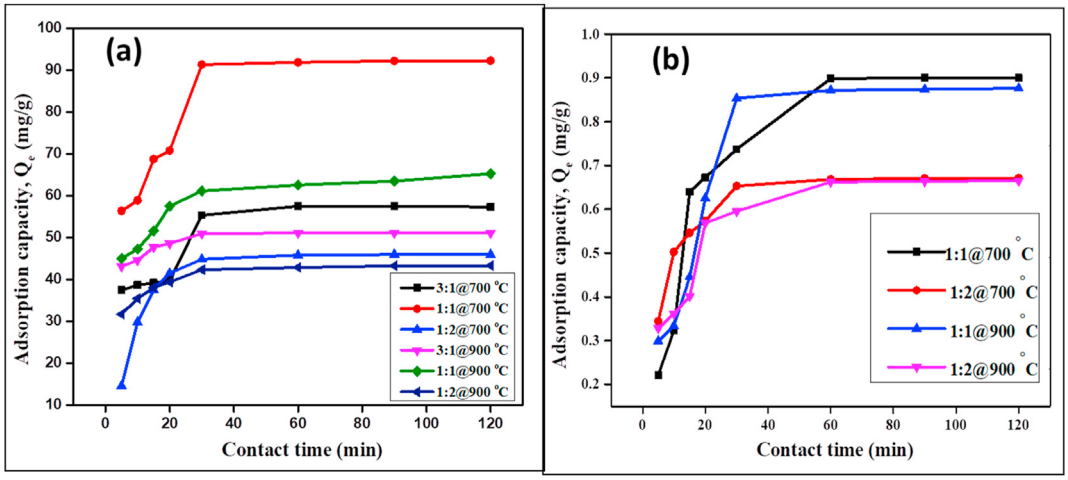

Fig. 6. Adsorption capacity for (a) TAN and (b) sulfide at different ratios of adsorbent mixture calcined at different temperatures.

R^2. The feasibility of adsorption was inferred by the values of the separation factor, R_L (Eq. (5)). Technically, if $R_L = 1$ (linear adsorption), $0 < R_L < 1$ (favorable adsorption) and $R_L > 1$ (unfavorable adsorption) [61]. The values of R_L for the removal of adsorbates were obtained in the range of −0.03 to −0.82 for TAN and −0.13 to −0.31 for sulfide. Since these values do not conform to the relation $0 < R_L < 1$, then it can be deduced that the uptake of both TAN and sulfide on AH@RR was not limited to a monolayer adsorption process and that the adsorption energy is not uniform for all sites. Hence, based on the values of R_L and the lower regression coefficients, it can be deduced that the Langmuir isotherm model cannot conveniently describe the adsorption of TAN and sulfide on the adsorbent used in this study.

The Freundlich adsorption model (Eqs. (6) and (7)) is valid for multilayer adsorption processes occurring due to the heterogeneity of the system. The linearized plots of log Q_e vs. log C_e shown in Fig. 8 were utilized to determine the values of parameters K_F and n (Table 4), which provide insight into the degree of adsorption and heterogeneity, respectively. The model also provides information about the degree of non-linearity between the adsorption and solution concentration. According to this model, the process is favorable if $1< n < 10$, but in cases when $n = 1$ and $n < 1$, it signifies linear and slow sorption processes, respectively [62]. The values of n obtained from this study were found to be less than 1, suggesting a slow uptake of TAN and sulfide from the liquid phase. In addition, the Freundlich isotherm does not predict the saturation of TAN and sulfide molecules on the surface of the adsorbent and thus reinforces the infinite coverage of the adsorbent surface [63]. Therefore, it is reasonable to deduce that the Freundlich model was not convenient to recount the adsorption of the two adsorbates

To further deduce the model fit to the experimental data, the Jovanovich adsorption model was tested and the results are summarized in Table 4. Plots of In Q_e vs. C_e (Fig. 9) were employed to obtain the isotherm parameters using equation (8). The data from the Jovanovich adsorption model seemed to fit better than all other models tested since the Jovanovich constant was in the favorable range of $0 < K_J < 1$ [64]. The fitting of this model was possible due to the existence of mechanical contacts between the adsorbent and adsorbate. This phenomenon is predisposed by the presence of carboxyl, hydroxyl, and amine groups derived from protein molecules present in the slaughterhouse waste [65,66]. The regression coefficients (R^2) of the Jovanovich model were very close to unity, ranging from 0.975 to 0.999, which were higher compared to the regression coefficients obtained from the Langmuir and Freundlich isotherms. It is apparent from our findings that the maximum adsorption capacities (qm, (mg/g)) for the Jovanovich model (Table 4) are higher than those obtained from Langmuir isotherms, making it more appropriate to adequately describe the adsorption of TAN and sulfide.

3.5. The effect of inorganic additives on methanogenesis

The effect of the adsorbent mixture in the reactor was evaluated in relation to the content of the biogas produced in the next 14 days after the addition of inorganic materials for the adsorption process. The adsorption process was carried out on day 44 after a tremendous decrease in the methane content by 36% from day 37. The effect of the added inorganic materials on methane production was assessed, in which the reactor with an additive mixture in a ratio of 1:2 showed an increase in the methane content by 13% in seven days (day 44–51) from 35.7 to 41.0% as indicated in Table 3. The trend was different from methane content recorded in the control reactors, in which there was a decrease in methane content from day 44 to 65. For instance, in reactor A, which was used for the control experiment (no adsorbent mixture was added), 24.6% of methane was produced on day 58 as opposed to 48.4% of methane content produced in reactor B. The trend further showed that the amount of methane in reactor B increased to 60.3% during day 65, while in the control reactor A, 22.8% of methane content was recorded on the same day.

Generally, the growth of methanogens in the AD system is highly influenced by trace elements such as Fe, Ni, and Co [67]. Therefore, the application of additives rich in iron such as iron oxides, ferric salts, and other iron-based materials is considered the best way to improve the methanogenesis process to its perfection and increase the methane content [68]. It is evident that the increase in methane content in this study was influenced by hematite (Fe_2O_3) present in the adsorbent mixture, which has the tendency of enhancing methanogenesis. The process is reinforced by ferric ion (Fe^{3+}) from hematite/magnetite present in the mixture of adsorbents, which is regarded as an electron acceptor and further oxidizes various organic substances through direct interspecies electron transfer from iron oxides [69]. This process is augmented by the exchange of electrons between fermenters and methanogens, which triggers the rapid degradation of the organic matter [68]. However, the addition of ferrous material during day 44 was a very crucial approach as it accelerated the increase of pH in the reactor from 7.24 (day 44) to 7.50 (day 65) as shown in Table 3. This condition resulted in mitigating the increase of volatile fatty acids and other intermediate products, which could further lead to severe stress of methanogens in the reactor, hence low methane content.

Table 4
Summarized isotherm parameters for the adsorption of TAN and sulfide onto the AH@RR adsorbent.

Isotherm parameters for TAN							Isotherm parameters for sulfide			
Temperature	700 °C			900 °C			700 °C		900 °C	
Adsorbent ratio (AH:RR)	3:1	1:1	1:2	3:1	1:1	1:2	1:1	1:2	1:1	1:2
Langmuir model										
q_m (mg/g)	35.34	43.70	8.67	35.99	23.65	17.05	0.19	0.29	0.25	0.28
k_L (L/mg)	−0.03	−0.006	−0.002	−0.02	−0.002	−0.003	−0.40	−0.66	−0.46	−0.79
R_L	−0.03	−0.18	−0.82	−0.05	−0.82	−0.43	−0.31	−0.16	−0.26	−0.13
R^2	0.998	0.985	0.910	0.998	0.991	0.990	0.897	0.952	0.938	0.978
Freundlich model										
$k_F[(mg/g)(L/mg)^{1/n}]$	184.98	3370	2×10^6	253.39	194×10^3	72×10^3	2.53	1.11	2.26	1.00
n	−3.87	−1.58	−0.57	−3.31	−0.79	−0.84	−0.99	−1.77	−1.09	−1.79
R^2	0.989	0.982	0.938	0.991	0.993	0.992	0.869	0.919	0.947	0.955
Jovanovich model										
q_m (mg/g)	63.96	144.44	179.93	64.64	196.80	124.62	1.67	0.96	1.53	0.91
K_J (L/g)	0.0012	0.0015	0.0026	0.0012	0.0021	0.0019	0.221	0.149	0.20	0.154
R^2	0.999	0.996	0.975	0.999	0.998	0.998	0.967	0.988	0.985	0.994

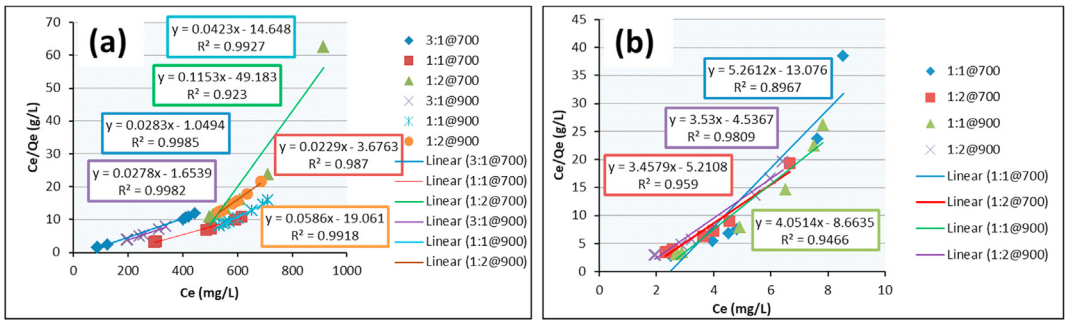

Fig. 7. Langmuir plots for (a) TAN and (b) sulfide removal.

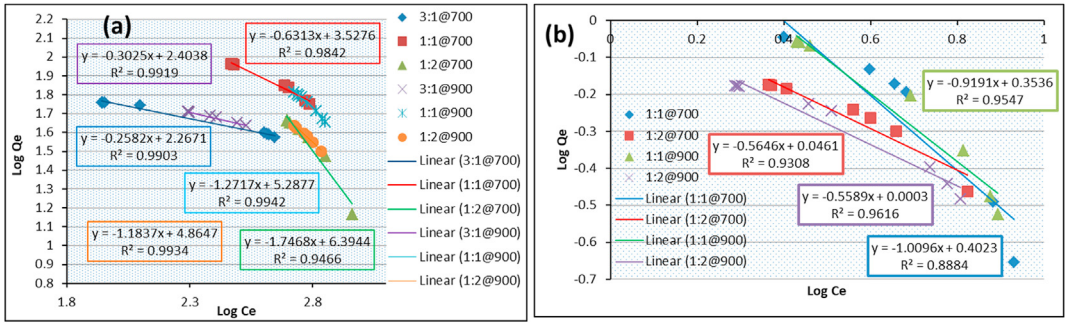

Fig. 8. Freundlich plots for (a) TAN and (b) sulfide removal.

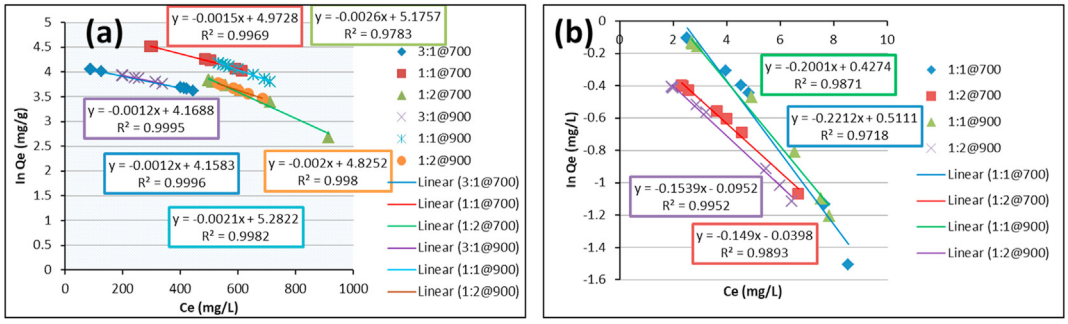

Fig.9. Jovanovich isotherms for (a) TAN and (b) sulfide removal.

4. Conclusions

The present study investigated the effect of mixing ratios of powdered adsorbent materials processed from the anthill and red rock soil samples in removing ammonia and sulfide in the liquid phase during AD of slaughterhouse waste. Analysis of the adsorbent's physicochemical characteristics was performed using p-XRD, FT-IR, porosimetry, and FE-SEM techniques. The highest surface area (852.8 m^2/g) and pore volume (0.75 cm^3/g) were displayed by the red rock soil sample calcined at 900 °C. Among all the adsorbent ratios investigated, the 3:1 ratio of the adsorbent calcined at both 700 and 900 °C showed a high removal efficiency for TAN (92%) while the ratio of 1:2 of the same adsorbent mixture under the same conditions was more efficient for sulfide removal (72%). Analysis of the adsorption isotherm models demonstrated that the Jovanovich model fitted better than the Langmuir and Freundlich models, with the Jovanovich constant in the range of $0 < K_J < 1$. Therefore, based on these findings, it can reasonably be concluded that anthill and red rock soils can be employed as affordable and effective adsorbents in the remediation of TAN and sulfide in the liquid phase as well as sustaining the methanogenesis process.

Authors contribution

All authors contributed to the study conception and design. Material preparation, data collection, and analysis were performed by Eric Mutegoa, Nyemaga Masanje Malima, Askwar Hilonga, and Karoli Njau. The first draft of the manuscript was written by Eric Mutegoa, and all authors commented on previous versions of the manuscript. All authors read and approved the final manuscript.

Declaration of competing interest

The authors declare that they have no known competing financial interests or personal relationships that could have appeared to influence the work reported in this paper.

Acknowledgement

The authors would like to acknowledge the African Centre of Excellence through WISE (Water Infrastructures and Sustainable Energy) – Futures Project at The Nelson Mandela African Institution of Science and Technology(NM-AIST), Tanzania for financial support.

References

[1] Q. Zhang, J. Hu, D.-J. Lee, Biogas from anaerobic digestion processes: research updates, Renew. Energy 98 (2016) 108–119, https://doi.org/10.1016/j.renene.2016.02.029.
[2] P.G. Kougias, I. Angelidaki, Biogas and its opportunities—a review, Front. Environ. Sci. Eng. 12 (2018) 14, https://doi.org/10.1007/s11783-018-1037-8.
[3] B. Bharathiraja, T. Sudharsana, J. Jayamuthunagai, R. Praveenkumar, S. Chozhavendhan, J. Iyyappan, Biogas production–A review on composition, fuel properties, feed stock and principles of anaerobic digestion, Renew. Sustain. Energy Rev. 90 (2018) 570–582, https://doi.org/10.1016/j.rser.2018.03.093.
[4] J. Kim, H. Kim, G. Baek, C. Lee, Anaerobic co-digestion of spent coffee grounds with different waste feedstocks for biogas production, Waste Manag. 60 (2017) 322–328, https://doi.org/10.1016/j.wasman.2016.10.015.
[5] Y. Ma, Y. Yin, Y. Liu, A holistic approach for food waste management towards zero-solid disposal and energy/resource recovery, Bioresour. Technol. 228 (2017) 56–61, https://doi.org/10.1016/j.biortech.2016.12.090.
[6] R. Cheerawit, T. Thunwadee, K. Duangporn, R. Tanawat, K. Wichuda, A. Niyi, A. Azhar, A.S. Ca, J. Victor, A. Nor Hasyimah, Biogas production from co-digestion of domestic wastewater and food waste, Health Environ. J. 3 (2012) 1–9.
[7] R. Li, Z. Zhi, H. Wang, Influence of carbon/nitrogen ratio on the anaerobic fermentative hydrogen production with cow dung compost, J. Renew. Sustain. Energy 6 (2014), 033139, https://doi.org/10.1063/1.4885615.
[8] D. Yadav, L. Barbora, L. Rangan, P. Mahanta, Tea waste and food waste as a potential feedstock for biogas production, Environ. Prog. Sustain. Energy 35 (2016) 1247–1253, https://doi.org/10.1002/ep.12337.
[9] M. Shahbaz, M. Ammar, D. Zou, R.M. Korai, X. Li, An insight into the anaerobic co-digestion of municipal solid waste and food waste: influence of co-substrate mixture ratio and substrate to inoculum ratio on biogas production, Appl. Biochem. Biotechnol. 187 (2019) 1356–1370, https://doi.org/10.1007/s12010-018-2891-3.
[10] Z. Zahan, S. Georgiou, T.H. Muster, M.Z. Othman, Semi-continuous anaerobic co-digestion of chicken litter with agricultural and food wastes: a case study on the effect of carbon/nitrogen ratio, substrates mixing ratio and organic loading, Bioresour. Technol. 270 (2018) 245–254, https://doi.org/10.1016/j.biortech.2018.09.010.
[11] I. Moukazis, F.-M. Pellera, E. Gidarakos, Slaughterhouse by-products treatment using anaerobic digestion, Waste Manag. 71 (2018) 652–662, https://doi.org/10.1016/j.wasman.2017.07.009.
[12] X. Wang, L. Zhang, B. Xi, W. Sun, X. Xia, C. Zhu, X. He, M. Li, T. Yang, P. Wang, Biogas production improvement and C/N control by natural clinoptilolite addition into anaerobic co-digestion of Phragmites australis, feces and kitchen waste, Bioresour. Technol. 180 (2015) 192–199, https://doi.org/10.1016/j.biortech.2014.12.023.
[13] S. Bwatota, M. Makungu, H. Nonga, Occurrences of indigestible foreign bodies in cattle slaughtered at Morogoro Municipal Slaughterhouse, Tanzania, J. Vet. Med. 2018 (2018).
[14] Á. Rodríguez-Abalde, X. Flotats, B. Fernández, Optimization of the anaerobic co-digestion of pasteurized slaughterhouse waste, pig slurry and glycerine, Waste Manag. 61 (2017) 521–528, https://doi.org/10.1016/j.wasman.2016.12.022.
[15] O. Córdova, J. Santis, G. Ruiz-Fillipi, M.E. Zuñiga, F.G. Fermoso, R. Chamy, Microalgae digestive pretreatment for increasing biogas production, Renew. Sustain. Energy Rev. 82 (2018) 2806–2813, https://doi.org/10.1016/j.rser.2017.10.005.
[16] E. Mutegoa, I. Kandola, A. Hilonga, K.N. Njau, Evaluating the Level of Ammonia and Sulfide in the Liquid Phase during Anaerobic Digestion of Slaughterhouse Waste Operating at Mesophilic Scale Digester—The Impact of Inhibition and Process Performance, 2020, https://doi.org/10.3934/energy.2020.4.615.
[17] P. Bin, R. Huang, X. Zhou, Oxidation resistance of the sulfur amino acids: methionine and cysteine, BioMed Res. Int. 2017 (2017), https://doi.org/10.1155/2017/9584932.
[18] H. Wang, I.A. Fotidis, I. Angelidaki, Ammonia–LCFA synergetic co-inhibition effect in manure-based continuous biomethanation process, Bioresour. Technol. 209 (2016) 282–289, https://doi.org/10.1016/j.biortech.2016.03.003.
[19] H. Huang, B.K. Biswal, G.-H. Chen, D. Wu, Sulfidogenic anaerobic digestion of sulfate-laden waste activated sludge: evaluation on reactor performance and dynamics of microbial community, Bioresour. Technol. 297 (2020) 122396, https://doi.org/10.1016/j.biortech.2019.122396.
[20] Y. Ding, M. Sartaj, Optimization of ammonia removal by ion-exchange resin using response surface methodology, Int. J. Environ. Sci. Technol. 13 (2016) 985–994, https://doi.org/10.1007/s13762-016-0939-x.
[21] F. Al-Sheikh, C. Moralejo, M. Pritzker, W.A. Anderson, A. Elkamel, Batch adsorption study of ammonia removal from synthetic/real wastewater using ion exchange resins and zeolites, Separ. Sci. Technol. (2020) 1–12, https://doi.org/10.1080/01496395.2020.1718706.
[22] R.Ö. Sürmeli, A. Bayrakdar, R. Molaey, B. Çalli, Synergistic effect of sulfide and ammonia on anaerobic digestion of chicken manure, Waste Biomass Valorization 10 (2019) 609–615, https://doi.org/10.1007/s12649-017-0090-z.
[23] E. Mutegoa, A. Hilonga, K.N. Njau, Approaches to the mitigation of ammonia inhibition during anaerobic digestion–a review, Water Pract. Technol. 15 (2020) 1–20, https://doi.org/10.2166/wpt.2020.047.
[24] A. Nozhevnikova, M. Simankova, Y.V. Litti, Application of the microbial process of anaerobic ammonium oxidation (ANAMMOX) in biotechnological wastewater treatment, Appl. Biochem. Microbiol. 48 (2012) 667–684, https://doi.org/10.1134/S0003683812080042.
[25] R. Machunda, T. Pogrebnaya, Removal of hydrogen sulfide from biogas using a red rock, J. Energy 2020 (2020), https://doi.org/10.1155/2020/2309378.
[26] C.P. Bergmann, F.M. Machado, Carbon Nanomaterials as Adsorbents for Environmental and Biological Applications, Springer, 2015, https://doi.org/10.1007/978-3-319-18875-1.
[27] K. Hina, M. Hedley, M. Camps-Arbestain, J. Hanly, Comparison of pine bark, biochar and zeolite as sorbents for NH4+-N removal from water, CLEAN–soil, Air, Water 43 (2015) 86–91, https://doi.org/10.1002/clen.201300682.
[28] P. Janetaisong, V. Lailuck, S. Supasitmongkol, Pelletization of iron oxide based sorbents for hydrogen sulfide removal, in: Key Engineering Materials, Trans Tech Publ, 2017, pp. 449–454, https://doi.org/10.4028/www.scientific.net/KEM.751.449.
[29] A.Ž. Gotvajn, T. Tišler, J. Zagorc-Končan, Comparison of different treatment strategies for industrial landfill leachate, J. Hazard Mater. 162 (2009) 1446–1456, https://doi.org/10.1016/j.jhazmat.2008.06.037.
[30] D.M. Cristiano, R.d.A. Mohedano, W.C. Nadaleti, A.B. de Castilhos Junior, V.A. Lourenço, D.F. Gonçalves, P. Belli Filho, H2S Adsorption on Nano-structured Iron Oxide at Room Temperature for Biogas Purification: Application of Renewable Energy, Renewable Energy, 2020, https://doi.org/10.1016/j.renene.2020.02.054.
[31] M. Šiljeg, L. Foglar, M. Kukučka, The ground water ammonium sorption onto Croatian and Serbian clinoptilolite, J. Hazard Mater. 178 (2010) 572–577, https://doi.org/10.1016/j.jhazmat.2010.01.123.
[32] A. APHA, Standard Methods for Examination of Water and Wastewater, American Public Health Association, Washington, 2015, ISBN 978-087553-013-0, p. 1360.
[33] S. Grimberg, D. Hilderbrandt, M. Kinnunen, S. Rogers, Anaerobic digestion of food waste through the operation of a mesophilic two-phase pilot scale digester–assessment of variable loadings on system performance, Bioresour. Technol. 178 (2015) 226–229, https://doi.org/10.1016/j.biortech.2014.09.001.
[34] V. Mota, F. Santos, T. Araújo, M. Amaral, Evaluation of titration methods for volatile fatty acids measurement: effect of the bicarbonate interference and feasibility for the monitoring of anaerobic reactors, Water Pract. Technol. 10 (2015) 486–495, https://doi.org/10.2166/wpt.2015.056.
[35] J. Harwood, A. Kühn, A colorimetric method for ammonia in natural waters, Water Res. 4 (1970) 805–811, https://doi.org/10.1016/0043-1354(70)90037-0.
[36] A. Strocchi, J.K. Furne, M.D. Levitt, A modification of the methylene blue method to measure bacterial sulfide production in feces, J. Microbiol. Methods 15 (1992) 75–82, https://doi.org/10.1016/0167-7012(92)90071-B.
[37] E.N. Richard, A. Hilonga, R.L. Machunda, K.N. Njau, A review on strategies to optimize metabolic stages of anaerobic digestion of municipal solid wastes towards enhanced resources recovery, Sustain. Environ. Res. 29 (2019) 36, https://doi.org/10.1186/s42834-019-0037-0.
[38] M.A. Al-Ghouti, D.A. Da'ana, Guidelines for the use and interpretation of adsorption isotherm models: a review, J. Hazard Mater. (2020) 122383, https://doi.org/10.1016/j.jhazmat.2020.122383.
[39] F. Al Jaberi, S. Jabbar, N. Jabbar, Modeling of adsorption isotherms of oil content through the electrocoagulation treatment of real oily wastewater, in: AIP Conference Proceedings, AIP Publishing LLC, 2020, 020041, https://doi.org/10.1063/5.0000157.
[40] A.F. Gualtieri, Accuracy of XRPD QPA using the combined Rietveld–RIR method, J. Appl. Crystallogr. 33 (2000) 267–278, https://doi.org/10.1107/S002188989901643X.
[41] M. Okui, H. Sawada, F. Marumo, Structure refinement of a nonstoichiometric pyroxene synthesized under ambient pressure, Phys. Chem. Miner. 25 (1998) 318–322.
[42] L. Levien, C.T. Prewitt, D.J. Weidner, Structure and elastic properties of quartz at pressure, Am. Mineral. 65 (1980) 920–930.
[43] N.L. Ross, J. Shu, R.M. Hazen, High-pressure crystal chemistry of stishovite, Am. Mineral. 75 (1990) 739–747.
[44] P. Fabrykiewicz, M. Stękiel, I. Sosnowska, R. Przeniosło, Deformations of the α-Fe2O3 rhombohedral lattice across the Néel temperature, Acta Crystallogr. B 73 (2017) 27–32, https://doi.org/10.1107/S2052520616017935.
[45] K. Ståhl, J.P. Legros, J. Galy, The crystal structure of SeO2 at 139 and 286 K, Z. für Kristallogr. – Cryst. Mater. 202 (1992) 99–107, https://doi.org/10.1524/zkri.1992.202.1-2.99.
[46]] R.M. Thompson, R.T. Downs, Model pyroxenes I: ideal pyroxene topologies, Am. Mineral. 88 (2003) 653–666, https://doi.org/10.2138/am-2003-0419.

[47] D.R. Peacor, High-temperature single-crystal study of the cristobalite inversion, Z. Kristallogr. 138 (1973) 274–298.
[48] J.G. Smith, Aspects of the loss-on-ignition (LOI) technique in the context of clay-rich, glaciolacustrine sediments, Geogr. Ann. Phys. Geogr. 85 (2003) 91–97, https://doi.org/10.1111/1468-0459.00191.
[49] S.P. Yeap, J. Lim, B.S. Ooi, A.L. Ahmad, Agglomeration, colloidal stability, and magnetic separation of magnetic nanoparticles: collective influences on environmental engineering applications, J. Nanoparticle Res. 19 (2017) 368, https://doi.org/10.1007/s11051-017-4065-6.
[50] T. Lu, J. Zhang, Y. Wei, P. Shen, Effects of ferric oxide on the microbial community and functioning during anaerobic digestion of swine manure, Bioresour. Technol. 287 (2019) 121393, https://doi.org/10.1016/j.biortech.2019.121393.
[51] G. Capson-Tojo, R. Moscoviz, S. Astals, Á. Robles, J.-P. Steyer, Unraveling the literature chaos around free ammonia inhibition in anaerobic digestion, Renew. Sustain. Energy Rev. 117 (2020) 109487, https://doi.org/10.1016/j.rser.2019.109487.
[52] J. Hu, J. Zhao, D. Wang, X. Li, D. Zhang, Q. Xu, L. Peng, Q. Yang, G. Zeng, Effect of diclofenac on the production of volatile fatty acids from anaerobic fermentation of waste activated sludge, Bioresour. Technol. 254 (2018) 7–15, https://doi.org/10.1016/j.biortech.2018.01.059.
[53] W. Zhang, S. Wu, J. Guo, J. Zhou, R. Dong, Performance and kinetic evaluation of semi-continuously fed anaerobic digesters treating food waste: role of trace elements, Bioresour. Technol. 178 (2015) 297–305, https://doi.org/10.1016/j.biortech.2014.08.046.
[54] A. Dar, U. Shafique, J. Anwar, M. Ali Munawar, Removal of sulfide ions from water using rice husk, J. Sulfur Chem. 36 (2015) 187–195, https://doi.org/10.1080/17415993.2015.1004067.
[55] K. Zhu, H. Fu, J. Zhang, X. Lv, J. Tang, X. Xu, Studies on removal of NH4+-N from aqueous solution by using the activated carbons derived from rice husk, Biomass Bioenergy 43 (2012) 18–25, https://doi.org/10.1016/j.biombioe.2012.04.005.
[56] D. Firer, E. Friedler, O. Lahav, Control of sulfide in sewer systems by dosage of iron salts: comparison between theoretical and experimental results, and practical implications, Sci. Total Environ. 392 (2008) 145–156, https://doi.org/10.1016/j.scitotenv.2007.11.008.
[57] M. Farghali, F.J. Andriamanohiarisoamanana, M.M. Ahmed, S. Kotb, T. Yamashiro, M. Iwasaki, K. Umetsu, Impacts of iron oxide and titanium dioxide nanoparticles on biogas production: hydrogen sulfide mitigation, process stability, and prospective challenges, J. Environ. Manag. 240 (2019) 160–167, https://doi.org/10.1016/j.jenvman.2019.03.089.
[58] D. Mohan, A. Sarswat, Y.S. Ok, C.U. Pittman Jr., Organic and inorganic contaminants removal from water with biochar, a renewable, low cost and sustainable adsorbent–a critical review, Bioresour. Technol. 160 (2014) 191–202, https://doi.org/10.1016/j.biortech.2014.01.120.
[59] B.N. Njoroge, S.G. Mwamachi, Ammonia removal from an aqueous solution by the use of a natural zeolite, J. Environ. Eng. Sci. 3 (2004) 147–154, https://doi.org/10.1139/s03-070.
[60] S. Ryskie, C. Gonzalez-Merchan, C.M. Neculita, T. Genty, Efficiency of ozone microbubbles for ammonia removal from mine effluents, Miner. Eng. 145 (2020) 106071, https://doi.org/10.1016/j.mineng.2019.106071.
[61] P. Baskaralingam, M. Pulikesi, D. Elango, V. Ramamurthi, S. Sivanesan, Adsorption of acid dye onto organobentonite, J. Hazard Mater. 128 (2006) 138–144, https://doi.org/10.1016/j.jhazmat.2005.07.049.
[62] S. Afroze, T.K. Sen, A review on heavy metal ions and dye adsorption from water by agricultural solid waste adsorbents, Water, Air, Soil Pollut. 229 (2018) 225, https://doi.org/10.1007/s11270-018-3869-z.
[63] N. Karapinar, R. Donat, Adsorption behaviour of Cu2+ and Cd2+ onto natural bentonite, Desalination 249 (2009) 123–129, https://doi.org/10.1016/j.desal.2008.12.046.
[64] T.A. Khan, S.A. Chaudhry, I. Ali, Equilibrium uptake, isotherm and kinetic studies of Cd (II) adsorption onto iron oxide activated red mud from aqueous solution, J. Mol. Liq. 202 (2015) 165–175, https://doi.org/10.1016/j.molliq.2014.12.021.
[65] R. Panahi, E. Vasheghani-Farahani, S. Shojosadati, Determination of adsorption isotherm for l-lysine imprinted polymer, Iran. J. Chem. Eng. 5 (2008) 49–55.
[66] M.A. Aly-Eldeen, A.A. El-Sayed, D.M. Salem, G.M. El Zokm, The uptake of Eriochrome Black T dye from aqueous solutions utilizing waste activated sludge: adsorption process optimization using factorial design, Egypt. J. Aquat. Res. 44 (2018) 179–186, https://doi.org/10.1016/j.ejar.2018.09.001.
[67] Y. Zhang, Z. Zhang, K. Suzuki, T. Maekawa, Uptake and mass balance of trace metals for methane producing bacteria, Biomass Bioenergy 25 (2003) 427–433, https://doi.org/10.1016/S0961-9534(03)00012-6.
[68] M. Wang, Z. Zhao, J. Niu, Y. Zhang, Potential of crystalline and amorphous ferric oxides for biostimulation of anaerobic digestion, ACS Sustain. Chem. Eng. 7 (2018) 697–708, https://doi.org/10.1021/acssuschemeng.8b04267.
[69] S.J. Kim, S.J. Park, I.T. Cha, D. Min, J.S. Kim, W.H. Chung, J.C. Chae, C.O. Jeon, S.K. Rhee, Metabolic versatility of toluene-degrading, iron-reducing bacteria in tidal flat sediment, characterized by stable isotope probing-based metagenomic analysis, Environ. Microbiol. 16 (2014) 189–204, https://doi.org/10.1111/1462-2920.12277.